

INHOMOGENEOUS FLUX PENETRATION IN NIOBIUM SHEET SAMPLED ACROSS THE CAVITY PRODUCTION ROUTE*

A. A. Polyanski[#], A. A. Squitieri, M. C. Jewell, P. J. Lee, A. Gurevich, D. C. Larbalestier, Applied Superconductivity Center, University of Wisconsin - Madison, Madison, WI, USA
P. Bauer, L. Bellantoni, C. Boffo, H. Edwards, Fermilab, Batavia, IL, USA

Abstract

Our initial studies of cavity-quality Nb prepared by buffered chemical polish (BCP) demonstrated that magneto-optical (MO) imaging could be used to show local flux penetration, some of which occurred preferentially at grain boundaries. In this new work, we have prepared small samples at each stage of processing associated with cavity production. The samples were machined from 2.8 mm thick sheet (RRR ~450). Samples from weld regions were compared to the regular samples. In addition to MO imaging, bulk magnetization was measured. Although large machining grooves were seen in all samples, topology was only intermittently seen in the MO images. Magnetization hysteresis associated both with surface and bulk pinning diminished through process but flux penetration became more inhomogeneous in the vicinity of H_{c1} for the more highly treated samples, especially the large-grain weld samples. Our results suggest that optimum treatments for the surface of Nb grains are not optimum for at least some Nb grain boundaries.

INTRODUCTION

In recent years it has become clear that superconducting Nb RF cavity performance is very sensitive to Nb surface quality and that careful surface preparation by buffered chemical polishing [1,2] or by electropolishing [3,4] followed by a low temperature bake is vital [5]. Gurevich [6] has recently proposed a model for Q drop triggered by early flux penetration, which makes local study of flux penetration very appropriate. In this new work we extend our first studies of flux penetration using magneto-optical imaging [7] to consider the role of Nb surface treatment in determining both global and local flux penetration.

EXPERIMENTAL TECHNIQUE

Magneto-optical imaging (MO) and Vibrating Sample Magnetometry (VSM) were used to study the local and global magnetization of samples machined from fine-grained Nb sheet (regular) and welded samples cut from the same sheet, both taken through a typical cavity optimization process. Grain size in the as-received sheet was ~50 μm , while the weld regions included grains larger than 1 mm. The samples were approximately $2.75 \times 2.75 \times 1.5$ mm in dimension. More details of the MO apparatus and technique are given in [7].

The processing sequence includes these 5 steps:

- (1) cold work produced by the sample machining process, followed by degreasing,
- (2) ~100 μm BCP etch,
- (3) 5 hours at 750°C in a vacuum $< 10^{-6}$ Torr,
- (4) ~20 μm BCP etch and
- (5) 50 hours at 120°C in a vacuum $< 10^{-6}$ Torr.

One sample in each condition was both MO imaged (see Fig. 1) and had a magnetization curve made, both measurements being performed at 7 K. This temperature was chosen so that the applied field in the MO cryostat could exceed the upper critical field (H_{c2}) of annealed, pure Nb at 7 K, ~110 mT [8].

RESULTS AND DISCUSSION

Figures 2 and 3 present VSM magnetization measurements on weld and regular samples after each step in the cavity optimization process. External field was applied perpendicular to the wide face of each sample in both experiments. Magnetization hysteresis is significantly reduced by the 100 μm BCP etch (curve 2), further reduced by the 750°C heat treatment (curve 3) and the subsequent etch (curve 4), but the final bake does not change the hysteresis for either the regular or weld samples. The removal of the cold work by the etch treatment (curve 2) is indicated by the large reduction in H_{c2} and by a small increase in the field of first flux penetration, approximately H_{c1} as the Ginzburg-Landau parameter κ is lowered to its annealed value found in the sheet center. The magnetization hysteresis cannot be unambiguously associated with either surface or bulk pinning from observing the global magnetization curves but MO imaging of the same sample can help elucidate the different contributions.

Figures 4 and 5 present a summary of a much larger image set taken at many fields for all regular and weld samples along the processing route. Optical images

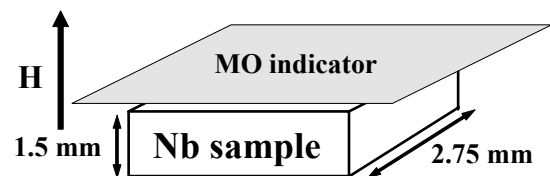


Figure 1: Geometry of the Magneto-optical experiment: The calculated sample demagnetization factor, $N=0.63$, and the maximum field enhancement ($2.7 H_{ext}$) is at the center of each side face when the Nb is fully diamagnetic.

* The work at UW-Madison was funded by FermiLab contract #559390 and DOE-HEP under grant DE-FG02-91 ER40643.

[#]polyansk@engr.wisc.edu

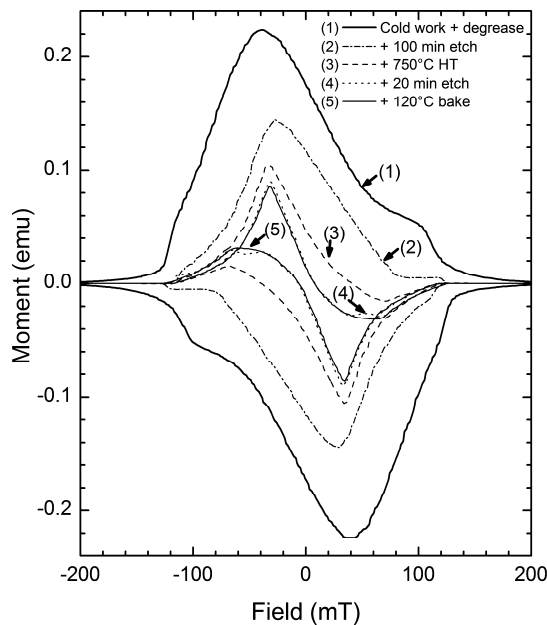


Figure 2: Magnetization curves taken on large-grain weld samples at 7 K for the whole process sequence.

clearly show coarse surface machining marks (row 1) that are somewhat smoothed after the BCP etching (conditions 2 and 4) for the small-grain, regular samples but are retained throughout processing in the weld samples. MO images taken at 7 K are shown in rows 2-4.

Row 4 in figures 4 and 5 show field cooled (FC) images. Evidence about the bulk pinning component of the hysteresis may be deduced from the images (row 4) made after cooling the samples in a field of 120 mT from above T_c to 7 K. The samples are then completely penetrated by field but, as the samples cool, defects capable of pinning flux become stronger and permit a bulk current density. Reducing the external field to zero at 7 K then establishes a roof pattern associated with such bulk screening current flow. These so-called field-cooled (FC) images of Figs 4 and 5 show quite strong roof-top patterns after steps 1 and 2 which progressively fade away through step 5. We interpret this weakening of the roof-top-pattern as showing that the bulk pinning component of the hysteresis is progressively reduced through the whole optimization sequence. Rather symmetric roof patterns are seen in the FC images of row 4, consistent with the hysteresis shown in Fig. 3, even in conditions 4 and 5. Symmetric rooftop patterns indicate homogenous bulk properties.

Evidence on the influence of the surface condition on flux penetration is better derived from the increasing field MO images. In all cases these images in rows 2 and 3 are less uniform after HT (step 3) than the remanent images shown in row 4. The regular samples in Fig. 5 do show the expected tendency for flux to enter along the center line of each face where the field enhancement is greatest. Comparing the lower field ZFC images in row 2 (set 3-5) to higher field images in row 3, it can also be seen that the pattern does become more regular after more flux has entered.

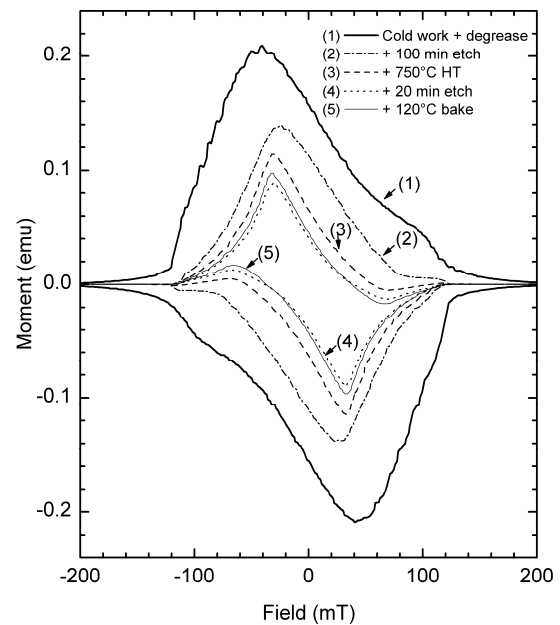


Figure 3: Magnetization curves taken on fine-grain regular samples at 7 K for the whole process sequence.

The weld samples show generally similar unstable behavior with two special features. The ZFC field images show distinctly non-uniform penetration after steps (1) and (2). After the 750°C heat treatment, flux penetration for fields just above H_{c1} ($H_{ext} \sim 30$ mT) becomes markedly more variable. Sudden and massive flux penetration from the center of each face is indicated in the sample 4 and 5 images, consistent both with the fact that the peak in the magnetization loops occurs at ~ 30 mT and that there is little bulk pinning to inhibit flux entry.

These significant changes in the MO images occur particularly strongly after the 20 min etch in step (4). This second chemical etch, which is believed to cause the grain boundaries to groove, promotes flux entry along grain boundaries in the large grain weld samples, as can be seen by comparing the MO and optical images. The grain boundaries visible in the MO images of the weld samples after steps 4 and 5 are direct evidence that the flux profile is being perturbed by the grain structure. Increasing the magnetic field (row 3 of figure. 4) leaves a cylinder of field within a still field-depleted ring near the edge that has lower energy than before flux entry. This flux entry occurred along one or more of the grain boundaries that are visible even through the machine marks visible on the weld samples 4 and 5.

Some perturbations to the FC MO images of the treatment 4 and 5 weld samples are consistent with perturbed properties of one or more of the Nb grain boundaries that are clearly visible in the optical and ZFC images.

As a whole the penetration is less uniform in the later treated samples and in the weld samples with large grains.

Finally we conclude that the reduction of hysteresis with increasing process step is due both to a reduction in bulk pinning as indicated by the bottom row FC images in figures 4 and 5 and by local surface pinning as indicated

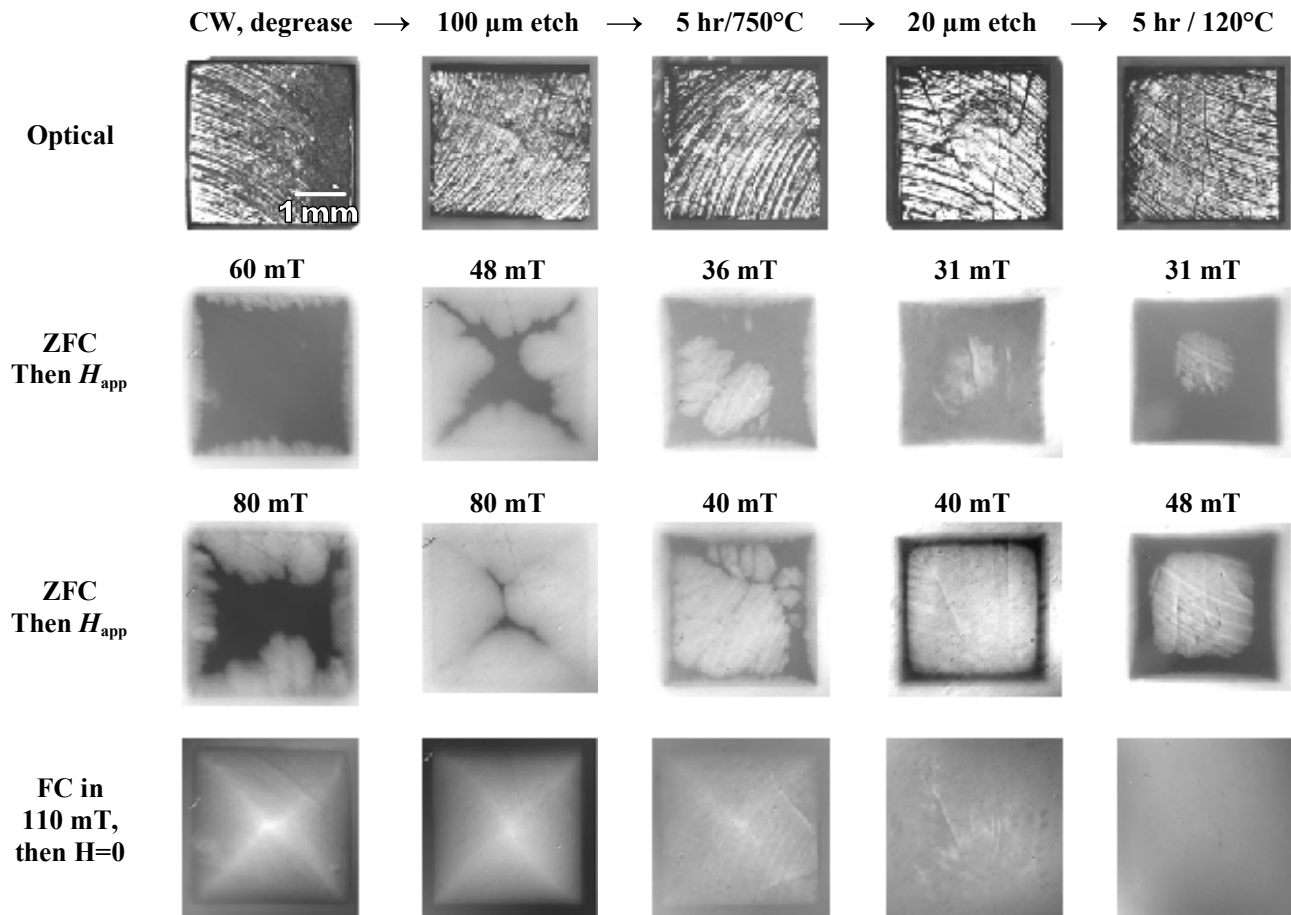


Figure 4: Optical and magneto-optical images of the weld (large grain) samples, taken sequentially after each process step. MO images were taken in the stated perpendicular external fields (H_{ext}).

by the column 4 and 5 ZFC images. More specific reasons for this behavior will be further investigated in the near future.

SUMMARY

1. The field-cooled, fully flux penetrated state is much more uniform than when field is applied from the ZFC state – the sample surface is clearly implicated for locally varying flux penetration in the superconducting state.
2. The “optimization” (etch, HT at 750°C, etch, bake) reduces global magnetization hysteresis, much of which comes from the surface, but enhances non-uniform flux penetration.
3. Flux penetration along grain boundaries is particularly apparent in the large grain weld samples.
4. Comparison of ZFC and FC images of the fully processed (120°C bake) weld samples shows perturbations of the local field in both cases – some GBs preferentially admit flux in the ZFC state and distort the induced current flow patterns which appear after reducing H to zero on FC.
5. Cavity performance is well known to improve after application of chemical etching processes similar to those used here. Our study does show that such treatments are capable of degrading grain boundary properties.

REFERENCES

- [1] Gmelin, Handbuch der anorganischen Chemie, Vol. 49(Nb), Springer, Berlin, 1970.
- [2] P. Kneisel, “Surface preparations of niobium”, M Kuntze (Ed.), Proceedings of the Workshop on RF Superconductivity, Vol. I + II, KFK, Karlsruhe, 1980, p. 27, KFK-3019.
- [3] K. Saito et al., “Superiority of electropolishing over chemical polishing on high gradients”, V. Palmieri (Ed.), Proceedings of the 8th Workshop on RF Superconductivity, Vol. I + II, INFN, Abano terme, 1997, pp. 759-813.
- [4] L. Lilje et al., Improved surface treatment of the superconducting TESLA cavities, Nucl. Instr. And Meth. A 516 (2-3) (2004) 213.
- [5] P. Kneisel, “Preliminary experience with in-situ baking of niobium cavities”, F. Krawczyk (Ed.), Proceedings of the 9th Workshop on RF Superconductivity, Vol. I + II, LANL, Santa Fe, 1999, pp. 77-91.
- [6] A. Gurevich, “Theoretical advances in SRF”, 12th International Workshop on RF Superconductivity, Cornell University, Ithaca, NY July 10-15, 2005.

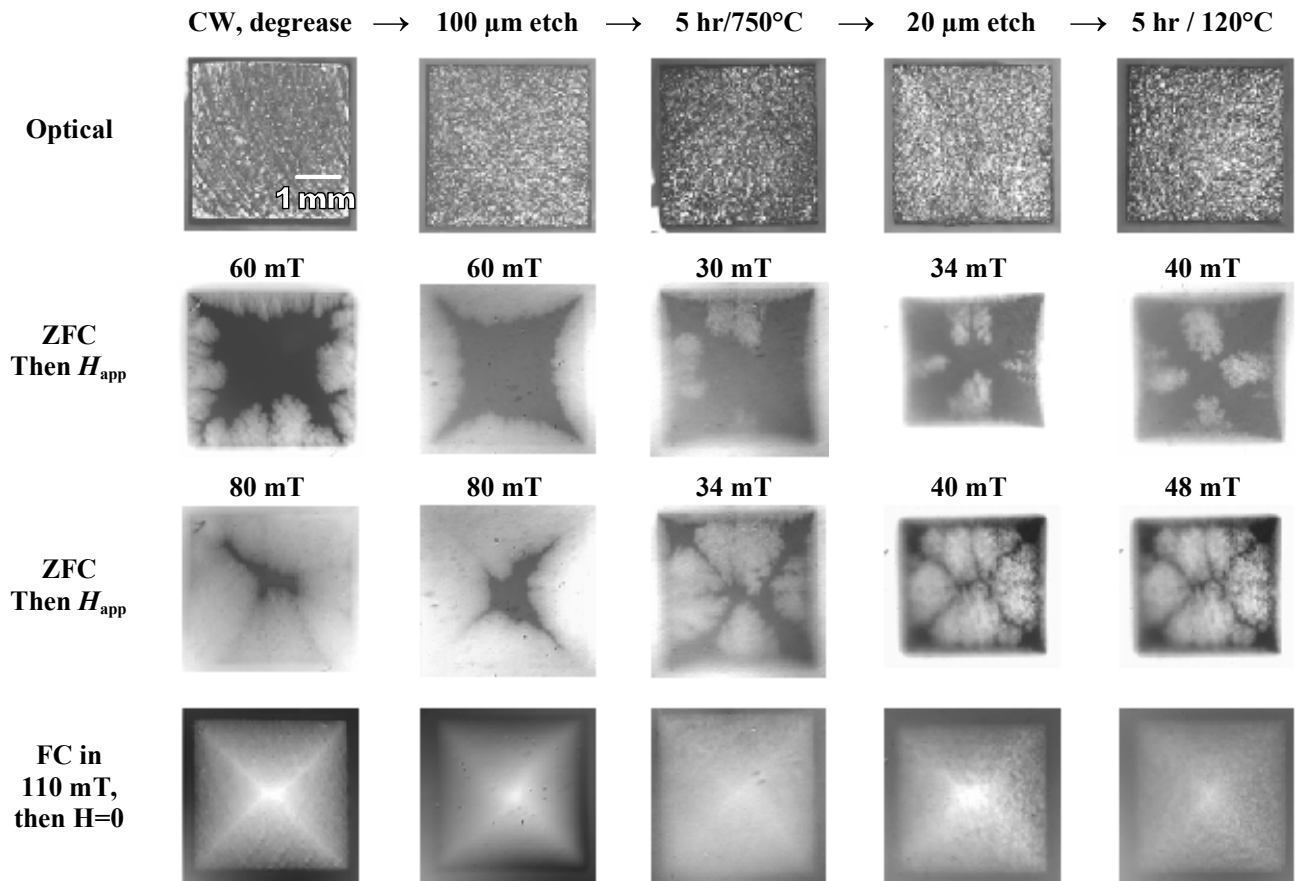


Figure 5: Optical and magneto-optical images of the regular (small grain) samples, taken sequentially after each process step. MO images were taken at the denoted external field (H_{ext}).

- [7] A. A. Polyanskii, D. M. Feldmann, and D. C. Larbalestier, "Magneto-Optical Characterization Techniques," "The Handbook on Superconducting Materials," Edited by David Cardwell and David Ginley, Institute of Physics UK, pp. 1551, 2003
- [8] K. Saito, "Fundamental RF Critical Field Overview", Pushing the Limits of RF Superconductivity

workshop, Argonne National Laboratory, September 22-24, 2004. Argonne National Laboratory Report ANL-05/10, Ed. Kwang-Je Kim and Catherine Eyberger, <http://www.aps.anl.gov/conferences/RFSC-Limits/ReadingMaterial.html>